2008 IEEE/RSJ International Conference on Intelligent Robots and Systems
Acropolis Convention Center
Nice, France, Sept, 22-26, 2008

Improvement of Dead Reckoning Accuracy of a Mobile Robot by Slip Detection and Compensation using Multiple Model Approach

Hyoung-Ki Lee, Kiwan Choi, Jiyoung Park, Yeon-Ho Kim, and Seokwon Bang

Abstract— Although dead reckoning based on odometry and inertial sensors is essential for a robotic localization system, none of previous works gives reliable and accurate position estimates on irregular terrain over long periods of time. Classical approaches use one estimator (such as a Kalman filter) with a single system model. However the single system model is not good to deal with both of slip and no-slip situations because of the dynamics changes. In this paper, a multiple model approach that uses two Kalman filters is presented: one Kalman filter accounting for no-slip condition and the other for slip condition. The Interacting Multiple Model (IMM) is adopted to switch two Kalman filters depending on whether slip occurs or not, and gives the weighted sum of two filter estimates. Experimental results are included to validate our approach.

I. INTRODUCTION

SAIT (Samsung Advanced Institute of Technology) has been developing cleaning robots for home environment, which can generate the coverage path and clean the floor minimizing the overlap of the traveled region. To meet this requirement, the robots need the capability of localization and map building. Simultaneous localization and map building algorithms are usually based on a Kalman filter or a particle filter which comprises two steps of prediction step and correction step [1]. In the prediction step, robot pose is estimated using odometry (such as wheel encoders) and in the correction step, the estimated robot pose is corrected by the measurement of other sensor signals. However, in home environment, a variety of obstacles such as books, rugs, and wires etc. on the floor cause the robot to slip and accumulate odometry errors. The odometry errors degrade the robot pose and map accuracies at the prediction step and make algorithms fail at worst.

Another problem for the cleaning robot in the home environment is immobilization. The cleaning robot is often tangled with electric wires or immobilized on rugs or doorsills. Autonomous robots should quickly detect the slip and immobilization in order to take appropriate actions, such as moving backward immediately and planning an alternative route to escape from the irregular terrain.

The researches on the slip detection and compensation can be categorized into two groups. One is exteroceptive method to utilize the absolute position measurement and the other is proprioceptive method to use only internal sensors like encoder, gyro, and accelerometer. In the field of exteroceptive method, Helmick et al. [2] proposed a system for the slip detection and compensation in a Mars rover based on visual odometry and inertial measurements through a Kalman filter. The combination of visual odometry with an absolute heading sensor was shown to be effective for robust long range navigation [3]. Absolute position measurements such as GPS make it simple to detect wheel slip and immobilization [4]. However, in all of the above exteroceptive methods, visual odometry is sensitive to illumination changes and GPS signal is not available in home environment. For those reasons, we will consider proprioceptive methods only in our paper.

In the field of proprioceptive method, wheel slip can be estimated through the use of encoders by comparing the speed of driven wheels with that of undriven wheels [5]. Ojeda and Borenstein proposed an indicator of wheel slip by comparing redundant wheel encoders against each other and again a yaw gyro [6]. These methods need redundant wheels and encoders. Ojeda and Borenstein also proposed another slip estimator based on motor current [7]. However this technique requires accurate current measurement and terrain specific parameter tuning. Ward and Iagnemma [8] proposed a model-based wheel slip detection by utilizing a tire traction/braking model and weak constraints for a Kalman filter.

To improve dead reckoning accuracy, many works have focused on calculating exact heading angle by utilizing gyroscopes and other sensors (such as a electronic compass or a tilt sensor) [9,10,11]. But these methods accumulate position error in the longitudinal direction of the robot. Barshan et al. proposed inertial navigation systems using error models of inertial sensors [12,13,14]. However the position estimation was reliable over only short period because of the accumulative errors of accelerometers. The sensor fusion of odometry and gyroscopes has been proposed in the frame of Kalman filtering to calculate the robot position and heading angle [15,16,17,18]. But, they are not applicable for navigation on

Manuscript received February 22, 2008.

Hyoung-Ki Lee is with the Micro Systems Lab., Samsung Advanced Institute of Technology, Yongin-Si, Gyeonggi-Do 449-712, South Korea (corresponding author to provide phone: +82-31-280-1761; fax: +82-31-280-9257; e-mail: twinclee@samsung.com).

Kiwan Choi is with the Micro Systems Lab., Samsung Advanced Institute of Technology, Yongin-Si, Gyeonggi-Do 449-712, South Korea (e-mail: kiwan@samsung.com).

Jiyoung Park is with the Micro Systems Lab., Samsung Advanced Institute of Technology, Yongin-Si, Gyeonggi-Do 449-712, South Korea (e-mail: ji.young.park@samsung.com).

Yeon Ho Kim is with the Micro Systems Lab., Samsung Advanced Institute of Technology, Yongin-Si, Gyeonggi-Do 449-712, South Korea (e-mail: ynho.kim@samsung.com).

Seokwon Bang is with the Micro Systems Lab., Samsung Advanced Institute of Technology, Yongin-Si, Gyeonggi-Do 449-712, South Korea (e-mail: banggar.bang@samsung.com).

irregular terrain because odometry gives false information when slip occurs. Reliable and accurate dead reckoning should be developed for the operation on irregular terrain over long periods of time.

All of the pervious works use one estimator (such as a Kalman filter) with a single system model regardless of whether slip occurs or not. However, we observed that two system models to treat no-slip and slip condition differently, should be introduced to improve dead reckoning accuracy because the kinematic model of a robot on normal floor is totally different from that on slippery floor.

To handle several parallel models, the IMM (Interacting Multiple Model) [19] and particle filter based algorithms were proposed. Zhang et al. [20] applied the IMM for fault detection and diagnosis, where the system structure and parameters change according to the occurrence of system failures. Freitas et al. [21] introduced an estimation technique to combine particle filters with Kalman filters for diagnosis in mobile robots. Plagemann et al. [22] applied techniques of Gaussian process classification and regression for learning proposal distributions of a particle filter to detect failures. The IMM is computationally more efficient than these sampling based techniques.

In this paper, a multiple model approach that uses two Kalman filters is proposed. In our approach, one Kalman filter accounts for no-slip condition and the other for slip condition. The IMM is adopted to give the automatic transition between them according to floor condition. The mode probability in the IMM works as an indicator of slippage and the final estimate of the IMM is a weighted sum of two Kalman filter estimates. In such a way, the IMM provides a unified approach for slip detection and compensation.

This paper is organized as follows. In section 2 we explain why multiple models are needed, and in section 3 two EKFs (Extended Kalman filters) relevant to slip condition are designed, and in section 4 our multiple model approach using the IMM is presented. In section 5 experimental results are presented. In section 6 conclusions are drawn from this work and future works are suggested.

II. NEED FOR MULTIPLE MODELS

The error covariance of odometry and accelerometer will be examined to explain the need for our multiple model approach. We consider a cleaning robot with differential drive kinematics (i.e., robots that have two independently driven wheels).

A. Properties of odometry errors

In case of no-slip, the relative position and orientation of the robot on even terrain can be modeled using odometry as follows:

$$\begin{bmatrix} x \\ y \\ \psi \end{bmatrix}_{k+1} = \begin{bmatrix} x \\ y \\ \psi \end{bmatrix}_{k} + \begin{bmatrix} \cos\psi_k \cdot \dfrac{(U_{R,k}+U_{L,k})}{2}(1+\Delta U) \\ \sin\psi_k \cdot \dfrac{(U_{R,k}+U_{L,k})}{2}(1+\Delta U) \\ \dfrac{(U_{R,k}-U_{L,k})}{D+\Delta D}(1+\Delta U) \end{bmatrix} \quad (1)$$

where x, y, and ψ are the relative position and orientation of the robot, $U_{R,k}$ and $U_{L,k}$ are the right and left wheel incremental distances, respectively, and D is the wheelbase of the robot. ΔU and ΔD represent systematic errors caused by the inaccurate modeling, limited system performance and so on [23].

For simplicity, we assume that the robot moves along the straight line then $U_{R,k} = U_{L,k}$ is obtained. The position error between the estimated and the real is given by $\delta x_k = \delta x_{k-1} + \Delta U \cdot U_{R,k}$.

Here ΔU is assumed to be white noise with $E(\Delta U^2) = \beta$. Then the variance of the position error is calculated by

$$E(\delta x_k^{\,2}) = \beta \sum_{i=1}^{k} U_{R,i}^2 .$$

When the robot moves with constant speed ($U_{R,i} = \alpha$), the above becomes

$$E(\delta x_k^2) = \alpha^2 \cdot \beta \cdot k . \quad (2)$$

The variance increases linearly proportional to time index k.

When the robot moves over uneven terrain and wheel slippage occurs, (1) is not applicable any more. The wheel slip, γ, can be defined as $\gamma = 1 - \dfrac{\upsilon}{R\omega_E}$, with υ as the linear speed of the wheel, R as wheel diameter, and ω_E as the angular rate of the wheel measured by encoders [7]. When $\gamma = 1$, the linear velocity is zero and the position error is given by $\delta x_k = \delta x_{k-1} + U_{R,k}$. The variance of position error is calculated as $E(\delta x_k^2) = (\sum_{i=1}^{k} U_{R,i})^2$. When the robot moves with constant speed ($U_{R,i} = \alpha$), the above becomes

$$E(\delta x_k^2) = \alpha^2 \cdot k^2 \quad (3)$$

Compared to the no-slip situation, the variance increases very rapidly because it is proportional to the square of k and $\beta \ll 1$.

B. Properties of accelerometer errors

Accelerometers measure the linear acceleration of the robot body. The position of the robot can be calculated by twice integration of it. But the position error increases rapidly with integration time and it needs other schemes like periodic absolute position sensing to reset the error. The position of the robot is given by $x_{k+1} = x_k + \upsilon_k \Delta t + \frac{1}{2} a_k \Delta t^2$

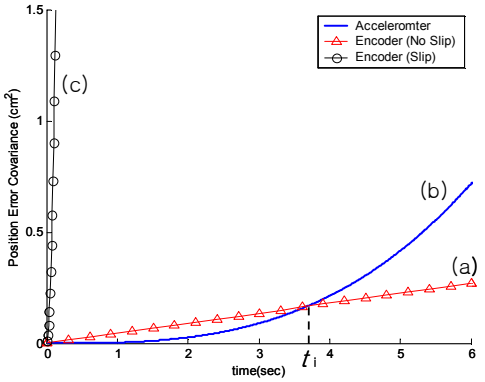

Fig. 1. Simulation result of position error variance

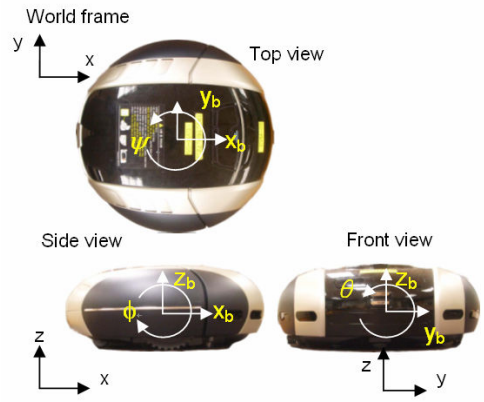

Fig. 2 . Cleaning robot and Euler angles

with $\upsilon_{k+1} = \upsilon_k + a_k \Delta t$, a_k as the linear acceleration, and Δt as the sampling time. White noise is assumed to be added to a_k . The variance of the position error is calculated by the followings:

$$E(\delta\upsilon_{k+1}^2) = E(\delta\upsilon_k^2) + E(\delta a_k^2)\Delta t^2$$

$$E(\delta x_{k+1}\delta\upsilon_{k+1}) = E(\delta x_k \delta\upsilon_k) + E(\delta\upsilon_k^2)\Delta t + E(\delta a_k^2)\frac{\Delta t^3}{2}$$

$$E(\delta x_{k+1}^2) = E(\delta x_k^2) + 2E(\delta x_k \delta\upsilon_k)\Delta t + E(\delta\upsilon_k^2)\Delta t^2 + E(\delta a_k^2)\frac{\Delta t^4}{4}$$

where δx , $\delta\upsilon$, and δa are the position error, velocity error, and accelerometer error, respectively. After kth integration, the position error variance becomes as follows:

$$E(\delta\upsilon_k^2) = k \cdot \Delta t^2 \cdot \sigma_a^2$$

$$E(\delta x_k \delta\upsilon_k) = \frac{k(k-1)}{2}\Delta t^3 \cdot \sigma_a^2$$

$$E(\delta x_k^2) = \frac{4k^3 - 6k^2 + 5k}{12}\Delta t^4 \cdot \sigma_a^2 \qquad (4)$$

where $E(\delta a_k^2) = \sigma_a^2$ and the initial variance at k=0 is assumed to be zero. Thus the variance increases in proportion to the cube of k .

C. *Introduction of multiple models*

Fig. 1 shows the exemplary simulation result of the position error variances of odometry and an accelerometer. In the simulation, (2), (3), and (4) were used assuming that the robot moves forward with the constant velocity ($\alpha = 30\text{cm/sec}$) and initial error covariance is zero. The sampling time Δt is 0.01sec and other simulation parameters are given by $\sigma_a = 1\text{cm}/\text{sec}^2$ and $\beta = 0.005\text{cm}^2$.

In case of no-slip, regarding the graph (a) and (b) of Fig. 1, the accelerometer has a smaller variance than the odometry until t_i and after t_i , the variance of the accelerometer increases very fast. To fuse data from two sensors, it is obvious that we should weigh more data of the accelerometer until t_i and weigh more data of the odometry after t_i . A Kalman filter performs this kind of sensor fusion optimally and efficiently.

In case of slip, regarding the graph (b) and (c) of Fig. 1, the odometry data has too large variance compared to the accelerometer data. So the data fusion of two sensors based on Kalman filter can't expect the performance improvement contrary to the case of no-slip. And it should be noticed that the expectation of the odometry error is not zero in the slip situation, thus it violates the assumption of zero mean white noise of Kalman filters.

From the above observation, we conclude that conventional Kalman filters using one system model is not good to deal with both of the slip and no-slip situations. In this paper, we propose a new method to use two system models and switch them according to the condition of slip or no-slip.

III. Extended Kalman Filter Design

A. *Robot Kinematic Model*

The robot moving on the irregular floor of home environments involves the attitude change. The attitude of a robot is a set of three angles measured between the robot's body and the absolute world coordinate frame. The body frame can be thought of as embedded in the robot body so that its x-axis points forward, the y-axis points to the left, and the z-axis points upward. The body axes are labeled x_b, y_b, and z_b. Referring to Fig. 2, three Euler angles, roll θ, pitch ϕ and yaw ψ are defined. To deal with the general three dimensional motion on the irregular floor, (1) should be extended to account for the tilt of the robot, which will be explained below in detail. The EKF for no-slip condition is designed to fuse data from encoders and inertial sensors, and the one for slip condition utilizes only inertial sensors.

B. *EKF for No-slip Condition*

There are two basic process models in a Kalman filter. The first is the system prediction describing how the state vector changes in time. The second is the measurement model which defines the relationship between the state vector and any measurement processed by the filter. As shown by graph (a) and (b) in Fig. 1, two data from encoders and accelerometers

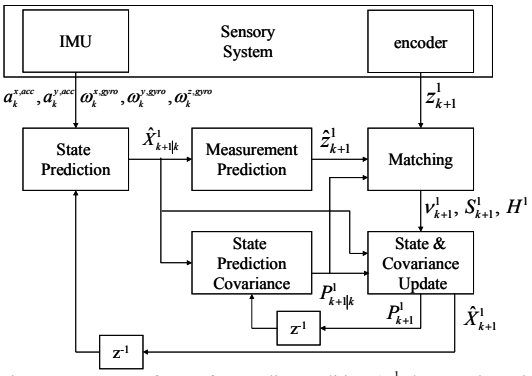

Fig. 3. Structure of EKF for no-slip condition (z^{-1} denotes the unit delay operator)

can complement each other by sensor fusion. Fig. 3 shows the structure of the EKF for no-slip condition. This EKF represents the mode 1 of the IMM.

a. Prediction model

To describe the 3-D motion of the robot, the state vector is defined as $X^1 = (x, y, \upsilon^x, a^x, \upsilon^y, a^y, \psi, \phi, \theta, \omega^z, \omega^y, \omega^x)^T$. The inputs of the system are $u_k^1 = (a_k^{x,acc}, a_k^{y,acc}, \omega_k^{x,gyro}, \omega_k^{y,gyro}, \omega_k^{z,gyro})^T$ where $a_k^{x,acc}$ and $a_k^{y,acc}$ are the mean robot accelerations along x_b and y_b axis measured by the accelerometer and $\omega_k^{x,gyro}, \omega_k^{y,gyro}$ and $\omega_k^{z,gyro}$ are the mean angular rates measured by the gyro during the *k*-th sampling interval. The superscript "1" of X^1 and u_k^1 denotes the mode 1 of the IMM. The state equation for the robot motion $X_{k+1}^1 = f^1(X_k^1, u_k^1) + \xi^1$ is

$$
\begin{aligned}
x_{k+1} &= x_k + (\upsilon_k^x \Delta t + \tfrac{1}{2} a_k^x \Delta t^2)\cos(\tilde{\psi}_k)\cos(\tilde{\phi}_k) \\
&\quad - (\upsilon_k^y \Delta t + \tfrac{1}{2} a_k^y \Delta t^2)\sin(\tilde{\psi}_k)\cos(\tilde{\theta}_k) + \xi_1^1 \\
y_{k+1} &= y_k + (\upsilon_k^x \Delta t + \tfrac{1}{2} a_k^x \Delta t^2)\sin(\tilde{\psi}_k)\cos(\tilde{\phi}_k) \\
&\quad + (\upsilon_k^y \Delta t + \tfrac{1}{2} a_k^y \Delta t^2)\cos(\tilde{\psi}_k)\cos(\tilde{\theta}_k) + \xi_2^1 \\
\upsilon_{k+1}^x &= \upsilon_k^x + a_k^x \Delta t + \xi_3^1 \\
a_{k+1}^x &= a_k^{x,acc} + |g|\sin(\tilde{\phi}_k) + \xi_4^1 \\
\upsilon_{k+1}^y &= \upsilon_k^y + a_k^y \Delta t + \xi_5^1 \\
a_{k+1}^y &= a_k^{y,acc} - |g|\cos(\tilde{\phi}_k)\sin(\tilde{\theta}_k) + \xi_6^1 \\
\omega_{k+1}^z &= \omega_k^{z,gyro} + \xi_{10}^1 \\
\omega_{k+1}^y &= \omega_k^{y,gyro} + \xi_{11}^1 \\
\omega_{k+1}^x &= \omega_k^{x,gyro} + \xi_{12}^1
\end{aligned}
\qquad (5)
$$

where $\tilde{\psi}_k = (\psi_k + \psi_{k+1})/2$, $\tilde{\phi}_k = (\phi_k + \phi_{k+1})/2$, and $\tilde{\theta}_k = (\theta_k + \theta_{k+1})/2$ are the average vehicle angles during the sampling interval Δt; ξ^1 is a white noise process vector with its covariance matrix Q^1; ξ_i^1 is the i-th element of vector ξ^1; |g| is the magnitude of gravity.

A simple method to calculate the Euler angles at time k+1 is as follows:

$$(\psi_{k+1}, \phi_{k+1}, \theta_{k+1})^T = (\psi_k, \phi_k, \theta_k)^T + (\omega_k^x \Delta t, \omega_k^y \Delta t, \omega_k^z \Delta t)^T \qquad (6)$$

But this method accumulates much numerical integration errors. It is known that the numerical integration in the directional cosine matrix has better accuracy [24]. Thus we first transform the Euler angles $(\psi_k, \phi_k, \theta_k)^T$ to the direction cosine matrix C_k.

$$
C_k = \begin{bmatrix}
\cos\phi_k \cos\psi_k & -\cos\theta_k \cos\psi_k & \sin\theta_k \sin\psi_k \\
 & +\sin\theta_k \sin\phi_k \cos\psi_k & +\cos\theta_k \sin\phi_k \cos\psi_k \\
\cos\phi_k \sin\psi_k & \cos\theta_k \cos\psi_k & -\sin\theta_k \sin\psi_k \\
 & +\sin\theta_k \sin\phi_k \sin\psi_k & +\cos\theta_k \sin\phi_k \sin\psi_k \\
-\sin\phi_k & \sin\theta_k \cos\phi_k & \cos\theta_k \cos\phi_k
\end{bmatrix} \qquad (7)
$$

The updated C_{k+1} from time k to k+1 is

$$C_{k+1} = C_k A_k = \begin{bmatrix} c_{11} & c_{12} & c_{13} \\ c_{21} & c_{22} & c_{23} \\ c_{31} & c_{32} & c_{33} \end{bmatrix} \qquad (8)$$

The small angle rotation matrix A_k may be written as $A_k = [I + \delta\Psi]$,

where $\delta\Psi = \dfrac{\sin(|\boldsymbol{\omega}|\Delta t)}{|\boldsymbol{\omega}|}\Omega_k + \dfrac{(1-\cos(|\boldsymbol{\omega}|\Delta t))}{|\boldsymbol{\omega}|^2}\Omega_k^2$,

$\boldsymbol{\omega} = (\omega_k^x, \omega_k^y, \omega_k^z)^T$, $|\boldsymbol{\omega}| = \sqrt{(\omega_k^x)^2 + (\omega_k^y)^2 + (\omega_k^z)^2}$,

$$\Omega_k = \begin{bmatrix} 0 & -\omega_z^k & \omega_y^k \\ \omega_z^k & 0 & -\omega_x^k \\ -\omega_y^k & \omega_x^k & 0 \end{bmatrix}$$

Then, C_{k+1} is transformed back to the Euler angles, $(\psi_{k+1}, \phi_{k+1}, \theta_{k+1})$.

$$\psi_{k+1} = \arctan\left[\frac{c_{21}}{c_{11}}\right], \phi_{k+1} = \arcsin[-c_{31}], \theta_{k+1} = \arctan\left[\frac{c_{32}}{c_{33}}\right] \qquad (9)$$

b. Measurement model

The measurements available in real time for each sampling period are $z_k^1 = (\upsilon_k^{x,encoder}, \upsilon_k^{y,encoder}, \omega_k^{z,encoder})^T$. $\upsilon_k^{x,encoder}$ and $\upsilon_k^{y,encoder}$ are the encoder measurements of the velocity along x_b and y_b axis, and $\omega_k^{z,encoder}$ is the encoder measurement of the angular velocity around z_b axis. The Measurement equation is given by $z_k^1 = H^1 X_k^1 + \eta^1$, where η^1 is a white measurement noise process vector with its covariance matrix R^1.

$$
\begin{aligned}
\upsilon_k^{x,encoder} &= \upsilon_k^x + \eta_1^1 \\
\upsilon_k^{y,encoder} &= \upsilon_k^y + \eta_2^1 \\
\omega_k^{z,encoder} &= \omega_k^z + \eta_3^1
\end{aligned}
\qquad (10)
$$

where η_i^1 is the i-th element of vector η^1.

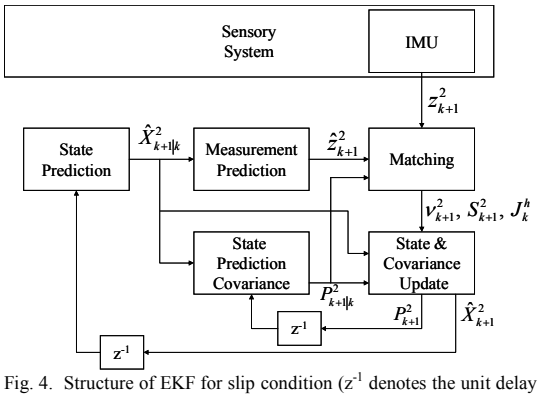

Fig. 4. Structure of EKF for slip condition (z^{-1} denotes the unit delay operator)

c. State estimate and covariance update

The EKF is used to correct the system prediction on the basis of the observations. The state prediction $\hat{X}^1_{k+1|k}$ at time k is $\hat{X}^1_{k+1|k} = f^1(\hat{X}^1_k, u^1_k)$ and the covariance matrix associated with the prediction error is written as

$$P^1_{k+1|k} = J^{f^1}_{X^1}(\hat{X}^1_k) P^1_k (J^{f^1}_{X^1}(\hat{X}^1_k))^T + Q^1 . \quad (11)$$

Here, $J^{f^1}_{X^1}(\cdot)$ is the Jacobian matrix of $f^1(\cdot)$ with respect to $\hat{X}^1_k$. The measurement prediction is $\hat{z}^1_{k+1} = H^1 \hat{X}^1_{k+1|k}$ and the final estimate is obtained as:

$$\hat{X}^1_{k+1} = \hat{X}^1_{k+1|k} + K^1_{k+1}[z^1_{k+1} - \hat{z}^1_{k+1}] \quad (12)$$

where the Kalman gain matrix is $K^1_{k+1} = P^1_{k+1|k} H^{1T} S^{1\ -1}_{k+1}$. The innovation covariance is $S^1_{k+1} = H^1 P^1_{k+1|k} H^{1T} + R^1$. The covariance associated with the final state estimate $\hat{X}^1_{k+1}$ is given by $P^1_{k+1} = P^1_{k+1|k} - K^1_{k+1} S^1_{k+1} K^{1T}_{k+1}$.

C. EKF for Slip Condition

In slip condition, the measurements from encoders give false information. So, we designed a Kalman filter without using the erroneous encoder signals. The prediction model is constructed using a dynamic model, and the measurement model using the signals from the IMU (Inertial Measurement Unit). Fig. 4 shows the structure of EKF for slip condition, which represents the mode 2 of the IMM. The designed filter can be regarded as a simplified version of the Kalman filter of ref. [12].

a. Prediction model

A state for slip condition is described by the following:

$$X^2 = (x, y, \upsilon^x, a^x, \upsilon^y, a^y, \psi, \phi, \theta, \omega^z, \omega^y, \omega^x, b^{ax}, b^{ay}, b^{\omega x}, b^{\omega y}, b^{\omega z})^T \quad (13)$$

where b^{ax} and b^{ay} are x and y axis biases of the accelerometer and $b^{\omega x}, b^{\omega y}$, and $b^{\omega z}$ are drift-rate biases of the gyros along x,y, and z axis, respectively. The above biases are slowly drifting signals and $\dot{b} = n_w$ is used to model these where n_w is a Gaussian white-noise process [15,25]. The state equations $X^2_{k+1} = f^2(X^2_{k+1}) + \xi^2$ are expressed by the following:

$$\begin{aligned}
x_{k+1} &= x_k + (\upsilon^x_k \Delta t + \tfrac{1}{2} a^x_k \Delta t^2)\cos(\tilde{\psi}_k)\cos(\tilde{\phi}_k) \\
&\quad - (\upsilon^y_k \Delta t + \tfrac{1}{2} a^y_k \Delta t^2)\sin(\tilde{\psi}_k)\cos(\tilde{\theta}_k) + \xi^1_1 \\
y_{k+1} &= y_k + (\upsilon^x_k \Delta t + \tfrac{1}{2} a^x_k \Delta t^2)\sin(\tilde{\psi}_k)\cos(\tilde{\phi}_k) \\
&\quad + (\upsilon^y_k \Delta t + \tfrac{1}{2} a^y_k \Delta t^2)\cos(\tilde{\psi}_k)\cos(\tilde{\theta}_k) + \xi^1_2 \\
\upsilon^x_{k+1} &= \upsilon^x_k + a^x_k \Delta t + \xi^2_3 \\
a^x_{k+1} &= a^x_k + \xi^2_4 \\
\upsilon^y_{k+1} &= \upsilon^y_k + a^y_k \Delta t + \xi^2_5 \\
a^y_{k+1} &= a^y_k + \xi^2_6 \\
\omega^z_{k+1} &= \omega^z_k + \xi^2_{10} \\
\omega^y_{k+1} &= \omega^y_k + \xi^2_{11} \\
\omega^x_{k+1} &= \omega^x_k + \xi^2_{12} \\
b^{ax}_{k+1} &= b^{ax}_k + \xi^2_{13} \\
b^{ay}_{k+1} &= b^{ay}_k + \xi^2_{14} \\
b^{\omega x}_{k+1} &= b^{\omega x}_k + \xi^2_{15} \\
b^{\omega y}_{k+1} &= b^{\omega y}_k + \xi^2_{16} \\
b^{\omega z}_{k+1} &= b^{\omega z}_k + \xi^2_{17}
\end{aligned} \quad (14)$$

The Euler angles, $(\psi_{k+1}, \phi_{k+1}, \theta_{k+1})$ can be calculated as mentioned above. In contrast to (5), (14) doesn't include the measurements from the inertial sensors as the system inputs.

b. Measurement model

The measurements from the IMU are utilized instead of encoder data. The measurement vector is

$$z^2_k = (a^{x,acc}_k, a^{y,acc}_k, \omega^{x,gyro}_k, \omega^{y,gyro}_k, \omega^{z,gyro}_k, \upsilon^{y,virtual}_k)^T \quad (15)$$

where $\upsilon^{y,virtual}_k$ is virtual measurement of the velocity along the y_b axis and should be approximately zero because the robot can't move along that direction. The measurement equation $z^2_k = h^2(X^2_k) + \eta^2$ is given by

$$\begin{aligned}
a^{x,acc}_k &= a^x_k - |g|\sin(\phi) + b^{ax}_k + \eta^2_1 \\
a^{y,acc}_k &= a^y_k - |g|\cos(\phi)\sin(\theta) + b^{ay}_k + \eta^2_2 \\
\omega^{x,gyro}_k &= \omega^x_k + b^{\omega x}_k + \eta^2_3 \\
\omega^{y,gyro}_k &= \omega^y_k + b^{\omega y}_k + \eta^2_4 \\
\omega^{z,gyro}_k &= \omega^z_k + b^{\omega z}_k + \eta^2_5 \\
\upsilon^{y,virtual}_k &= \upsilon^y_k + \eta^2_6
\end{aligned} \quad (16)$$

where η^2 is a white measurement noise process vector with its covariance matrix R^2.

The state estimate and covariance update are the same as the ones for normal operation. They will not be repeated here.

IV. A Multiple Model Approach for Slip Detection and Compensation

The above Kalman filters should be switched according to

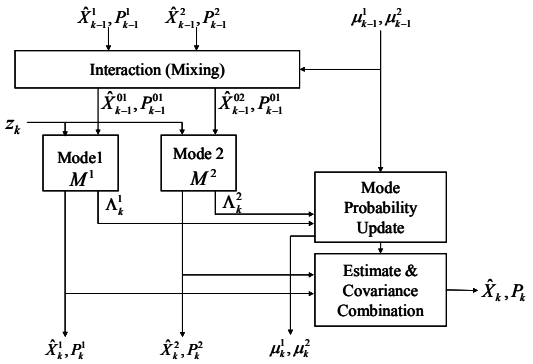

Fig. 5. Structure of the IMM with two modes

the occurrence of slip. For this purpose, we employed the IMM that is a well known method to deal with multiple system models. In our use of the IMM, mode 1 of the IMM accounts for no-slip condition, and mode 2 does for slip condition. In the frame of the IMM, transition between two modes is automatic.

Fig. 5 shows the architecture of the IMM algorithm used in our multiple model approach. In the figure, "Mode 1" is the EKF for no-slip condition and "Mode 2" is the EKF for slip condition. At each time k, a linear combination of the previous outputs (states and covariances, $\hat{X}^{0j}_{k-1}, P^{0j}_{k-1}$) is the input into each mode. Also, the current measurement, z_k is the input into each model and residuals are computed along with corresponding likelihood functions, Λ^j_k. Mode probabilities μ^j_k are used as weights in a linear combination of current model outputs to form the desired blended state and covariance outputs. The following shows one cycle of the IMM algorithm [26].

Step1: Calculation of the mixing probabilities

The probability that mode M^i was in effect at k-1 given that M^j is in effect at k conditioned on $Z_{k-1} \equiv \{z_i\}_{i=1}^{k-1}$ is

$$\mu^{i|j}_{k-1|k-1} \equiv P\{M^i_{k-1} \left| M^j_k, Z_{k-1}\right.\} = \frac{1}{\bar{c}_j} p_{ij} \mu^i_{k-1} \tag{17}$$

where the normalizing constants are $\bar{c}_j = \sum_{i=1}^{2} p_{ij} \mu^i_{k-1}$ and mode transition probability $p_{ij} \equiv P\{M^j_k \left| M^i_{k-1}\right.\}$, $i, j = 1$ or 2.

Step2: Interaction (Mixing)

Starting with $\hat{X}^i_{k-1}$, one computes the mixed initial condition for the filter matched to M^j_k as

$$\hat{X}^{0j}_{k-1} = \sum_{i=1}^{2} \hat{X}^i_{k-1} \mu^{i|j}_{k-1|k-1} \tag{18}$$

The covariance corresponding to the above is

$$P^{0j}_{k-1} = \sum_{i=1}^{2} \mu^{i|j}_{k-1|k-1} \left\{ P^i_{k-1} + \left[\hat{X}^i_{k-1} - \hat{X}^{0j}_{k-1}\right] \cdot \left[\hat{X}^i_{k-1} - \hat{X}^{0j}_{k-1}\right]^T \right\} \tag{19}$$

Step3: mode-matched filtering

The estimate $\hat{X}^{0j}_{k-1}$ and covariance P^{0j}_{k-1} are used as input to the filter matched to M^j_k, which uses z_k to yield $\hat{X}^j_k$ and covariance P^j_k. The likelihood functions corresponding to the two modes are as follows:

$$\Lambda^j_k \equiv p\left[z_k \mid M^j_k, Z_{k-1}\right] = N\left[z_k; \hat{z}^j_k, S^j_k\right] \tag{20}$$

where $N(\cdot)$ denotes the normal pdf with argument z_k, mean $\hat{z}^j_k$, and variance S^j_k.

Step4: Mode probability update

$$\mu^j_k \equiv P\{M^j_k \left| Z_k\right.\} = \frac{1}{c} \Lambda^j_k \cdot \bar{c}_j \tag{21}$$

where the normalization constant is $c = \sum_{j=1}^{2} \Lambda^j_k \cdot \bar{c}_j$

Step 5: Estimate and covariance combination

Combination of the model-conditioned estimates and covariances is done according to the mixture equations.

$$\begin{aligned} \hat{X}_k &= \sum_{j=1}^{2} \hat{X}^j_k \mu^j_k \\ P_k &= \sum_{j=1}^{2} \mu^j_k \left\{ P^j_k + \left[\hat{X}^j_k - \hat{X}_k\right] \cdot \left[\hat{X}^j_k - \hat{X}_k\right]^T \right\} \end{aligned} \tag{22}$$

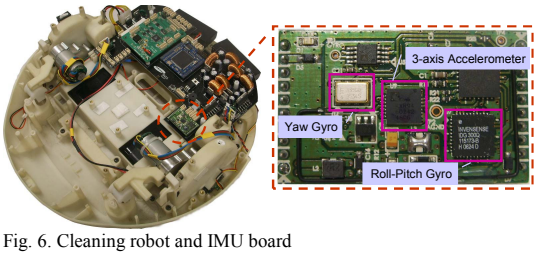

Fig. 6. Cleaning robot and IMU board

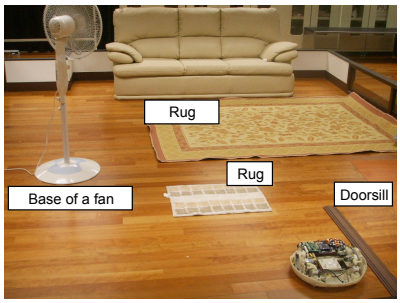

Fig. 7. Experimental environment setup

V. Experimental Results

The onboard sensory system includes two incremental encoders measuring the rotation of each motor, and an IMU that provides measures of the robot linear accelerations and angular rates. Fig. 6 shows the cleaning robot and custom-made IMU board. The IMU board has one yaw gyro (XV-3500, EPSON corporation), one roll-pitch gyro (IDG-300, Invensense, Inc.), one 3-axis accelerometer (KXPA4, Kionix, Inc.), and a microprocessor. The yaw gyro

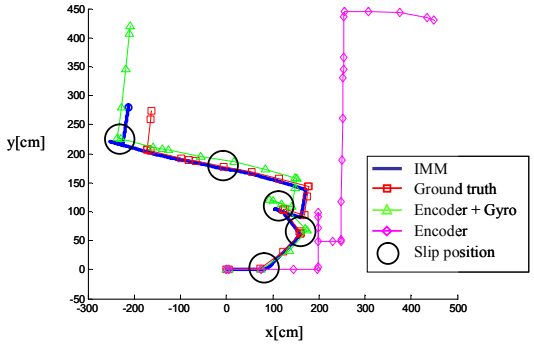

Fig. 8. Position trajectory after traveling for 80 seconds on the irregular floor

was calibrated on the self-made rate table to compensate for the scale factor nonlinearity. This calibration procedure is explained in [15] in more detail. The other sensors are used without calibration. The IMU board costs less than $20 to be cheap enough for cleaning robot products.

To verify the overall effectiveness of the proposed method, we performed some experiments on the irregular floor. Fig. 7 shows an experimental setup, which has a doorsill, rugs, and the base of a fan. The noise parameters of inertial sensors in the EKFs are experimentally determined and the other parameters are empirically determined. The mode transition probability of equation (17) is set $p_{11} = 0.99$, $p_{12} = 0.01$, $p_{21} = 0.005$, and $p_{22} = 0.995$. The robot starts to travel at position (0,0). The ground truth trajectory was measured by a motion tracker system (Hawk digital System, Motion Analysis, Inc.) and is shown in Fig. 8 with the label "Ground truth". In the figure, the label "Encoder" denotes the trajectory generated by only odometry. The label "Encoder+Gyro" represents the trajectory using a method presented by [15], where indirect Kalman filter fused the data from the encoders and a yaw gyro to calculate the heading angle. The trajectory represented

TABLE I
EXPERIMENTAL RESULTS [UNIT: CM,DEG]

Trial	Encoder		Encoder+Gyro		IMM	
	Position Error	Yaw Error	Position Error	Yaw Error	Position Error	Yaw Error
1	631.26	88.79	153.83	1.13	20.56	1.11
2	51.79	7.62	53.37	0.12	6.25	0.12
3	219.87	115.52	48.78	0.07	13.31	0.80
4	156.50	117.60	19.73	-0.12	6.01	0.53
5	135.92	26.75	90.24	1.48	27.16	1.52
6	154.37	19.91	110.40	1.25	1.34	1.09

by the label "IMM" shows a much less position error than that of the trajectory with the label "Encoder+Gyro", because it can compensate for the longitudinal distance error caused by slip. Both of the trajectory label with "Encoder+Gyro" and "IMM" show small errors in the heading. The trajectory labeled with "Slip position" shows the location where the slip occurred.

Fig. 9 shows the velocity profile and the mode 2 probability when the robot moves on the experimental setup. In the interval of "Stop", since the robot doesn't move, the biases of the gyros were reset the mean values of current gyro outputs to compensate for the bias drift. And mode 1 and mode 2 probability are set 0.5 because the stop mode doesn't belong either of mode 1 and mode 2. In the Fig. 9 (a), "IMM" has better tracking performance than "Encoder" in the presence of slip. Fig. 9 (b) shows the mode 2 probability, where it is near zero under no-slip condition and it approaches one when the slip occurs. It should be noted that mode 2 probability indicates the possibility of slip occurrence and can be used as a slip detection index.

We performed 6 sets of experiments on the irregular floor changing the location of obstacles. Table I summarizes the experimental results. The final position errors and yaw errors were recorded after the robot traversed for 80~120 seconds. The position error is the Euclidean distance of x and y direction errors and the yaw error is the absolute value of error between the ground truth and the estimated value. The posi-

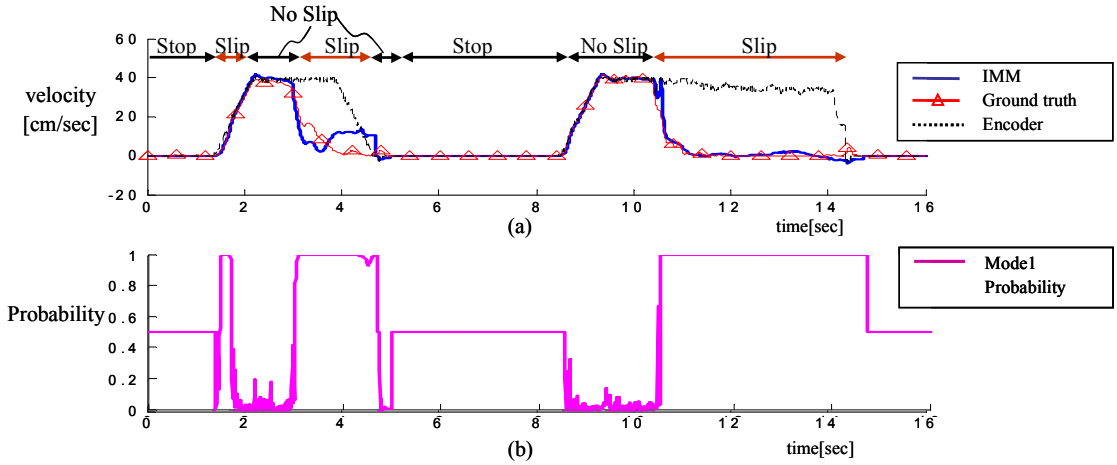

Fig. 9. Velocity profile and mode2 probability

tion errors of the IMM are much smaller than those of "Encoder+Gyro".

VI. Conclusions and Future Works

In this paper, we have presented a novel method for wheel-slip detection and compensation for cleaning robots to improve the dead reckoning performance. Dead reckoning is the key to simultaneous localization and map-building algorithms, because they have a prediction step to estimate the position of the robot resorting to dead reckoning. We designed a new multi model approach using two Kalman filters accounting for no-slip and slip condition. For this, an IMM structure was employed to switch two Kalman filters automatically according to the probability of the slip occurrence. In the IMM structure, mode 2 (slip mode) probability was used as a slip index to detect the slip. Experimental results were presented to show that our approach dramatically reduced the position error of the robot traveling on the floor with slip. As a future work, we will extend our approach by adding another "Stop" mode to correct the biases of inertial sensors more accurately when the robot stops.

References

[1] S. Thrun, W. Burgard, and D. Fox, *Probabilistic robotics*, The MIT Press, 2005, ch.10.

[2] D.M. Helmick, Y.Cheng, D.S. Clouse, M. Bajracharya, L.H. Matthies, and S.I. Roumeliotis, "Slip Compensation for a Mars Rover," in proc. IROS 2005, pp. 2806-2813.

[3] C.Olson, L. Matthies, M. Schoppers, and M. Maimone, "Robust stereo ego-motion for long distance navigation, " in Proc. of IEEE conf. on Computer Vision and Pattern Recognition, vol.2, 2000, pp. 453-458.

[4] S. Sukkarieh, E. Nebot, and H. F. Durrant-Whyte, "A high integrity IMU/GPS navigation loop for autonomous land vehicle applications," IEEE trans. on Robotics and Automation, vol.15, no.3, June 1999.

[5] F. Gustafsson,"Slip-based tire-road friction estimation," Automatica, vol.33, no.6, 1997, pp.1087-1099.

[6] L. Ojeda, G.Reina, and J.Borenstein, "Experimental results from FLEXnav: An expert rule-based dead-reckoning system for Mars rovers," IEEE Aerospace Conference 2004, Big Sky, MT, 2004.

[7] L. Ojeda, D. Cruz, G.Reina, and J.Borenstein,"Current-based slippage detection and odometry correction for mobile robots and planetary rovers," IEEE trans. on Robotics, vol.22, no.2, April 2006.

[8] C.C. Ward, K. Iagnemma, "Model-Based Wheel Slip Detection for Outdoor Mobile Robots", in proc. of ICRA 2007, pp. 2724 – 2729.

[9] M.Hoshino, Y. Gunji, S. Oho, and K. Takano, "A Kalman Filter to Estimate Direction for Automotive Navigation", in proc. of MFI 1996, pp. 145-150.

[10] S. I. Roumeliotis, G. S. Sukhatmae, and G. A. Bekey, "Circumventing Dynamic Modeling: Evaluation of the Error-State Kalman Filter applied to Mobile Robot Localization", in proc. of ICRA 1999, pp. 1656-1663.

[11] L. Ojeda and J. Borenstein, "FLEXnav: Fuzzy Logic Expert Rule-based Position Estimation for Mobile Robots on Rugged Terrain", in proc. of ICRA 2002, pp. 317-322.

[12] B. Barshan and H. F. Durrant-Whyte, "Inertial Navigation Systems for Mobile Robots", IEEE Trans. on Robotics and Automation, vol. 11, no. 3, 1995, pp. 328-342.

[13] B. Barshan and H. F. Durrant-Whyte, "Orientation Estimate for Mobile Robots using Gyroscopic Information", in proc. of IROS 1994, pp. 1867-1874.

[14] B. Barshan and H. F. Durrant-Whyte, "Evaluation of a Solid-State Gyroscope for Robotics Applications", IEEE trans. on Instrumentation and measurement, vol. 44, no. 1, 1994, pp.61-67.

[15] H. Myung, H.K. Lee, K. Choi, S. Bang, Y.B. Lee, and S.R. Kim, "Constrained Kalman Filter for Mobile Robot Localization with Gyroscope", in proc. of IROS 2006, pp. 442-447.

[16] H. Hardt, D. Wolf, and R. Husson, "The Dead Reckoning Localization System of the Wheeled Mobile Robot ROMANE", in proc. of MFI 1996, pp. 603-610.

[17] F. Azizi and N. Houshangi, "Mobile Robot Position Determination Using Data from Gyro and Odometry", in proc. of the Canadian Conf. on Electrical and Computer Engineering, 2004, pp. 719–722.

[18] H. Chung, L. Ojeda, and J. Borenstein, "Sensor fusion for Mobile Robot Dead-reckoning With a Precision-calibrated Fiber Optic Gyroscope", in proc. of ICRA 2001, pp.3588-3593.

[19] E. Mazor, A. Averbuch, Y. Bar-shalom, and J. Dayan, "Interactive multiple model methods in target tracking: a survey", IEEE trans. on Aerospace and Electronic Systems, vol.34, no.1, 1998, pp.103-123.

[20] Y. Zhang and J. Jiang, "Integrated Active Fault-Tolerant Control Using IMM Approach", IEEE trans. on Aerospace and Electronic Systems, vol.37, no.4, 2001, pp.1221-1235.

[21] N. de Freitas, R. Dearden, F. Hutter, R. Morales-menendez, J. Mutch, and D. Poole, "Diagnosis by a Waiter and a Mars Explorer", in proc. of the IEEE, vol. 92, no. 3, 2004, pp. 455-468.

[22] C. Plagemann, D. Fox, and W. Burgard, "Efficient Failure Detection on Mobile Robots Using Particle Filters with Gaussian Process Proposals", in proc. of IJCAI, 2007.

[23] J. Borenstein and L. Feng, "Gyrodometry: A New Method for Combining Data from Gyros and Odometry in Mobile Robots", in proc. of ICRA 1996, pp. 423-428.

[24] D. H. Titterton, J. L. Weston, *Strapdown inertial navigation technology -2nd edition,* The Institution of Electrical Engineers, 2004, ch.3.6.

[25] S. I. Roumeliotis, G. S. Sukhatme, and G. A. Bekey, "Circumventing Dynamic Modeling: Evaluation of the Error-State Kalman Filter applied to Mobile Robot Localization", in proc. of ICRA 1999, pp. 1656-1663.

[26] Y. Bar-Shalom, X. Li, and T. Kirubarajan, *Estimation with applications to tracking and navigation*, JOHN WILEY & SONS, INC, 2001, ch.11.